Penetration-depth calculations in the *ab* and *c* directions in a layered *S/N* superconductor

W. A. Atkinson and J. P. Carbotte
Department of Physics and Astronomy, McMaster University, Hamilton, Ontario, Canada L8S 4M1
(Received 31 October 1994)

We present the results of calculations of the penetration depths λ_{ab} and λ_c (the subscripts refer to the direction of the screening currents). Our model is a layered superconducting/normal metal (S/N) model, in which the two types of layers are stacked in alternating fashion. The S and N layers are coupled in a coherent fashion and the N layer is driven superconducting by a proximity effect. We calculate the penetration depths for both *d*-wave and *s*-wave order parameters for a range of interlayer coupling strengths, and we discuss the effect that the interlayer coupling has on the temperature dependence of the penetration depths. We finish by comparing our results with experimental observations of $YBa_2Cu_3O_7$.

I. INTRODUCTION

Recent measurements of the penetration depth of a magnetic field into high-temperature superconductors have sparked a great deal of interest. Hardy *et al.*[1] measured the in-plane penetration depth λ_{ab} of single crystals of $YBa_2Cu_3O_{6.95}$ and found that at low temperatures, $\lambda_{ab}(T)^{-2}$ obeys a linear law, rather than the T^2 law previously[2–4] found in thin-film samples. This evidence was taken as support for models in which the gap exhibits a node on the Fermi surface.[5] In particular, this data was found to be consistent with *d*-wave theories.[6,7] More recent work[8] on untwinned crystals of YBCO has found that the penetration depth is different if measured along the *a* axis and *b* axis. This is attributed to the existence of a large superfluid density on the copper-oxide chains. There has also been recent work[9,10] on single crystals of YBCO in which the penetration depth perpendicular to the copper-oxide planes λ_c was measured. The results of optical and infrared measurements presented in Ref. 9 show that, in contrast to the linear behavior of λ_{ab}^{-2}, the low-temperature dependence of λ_c^{-2} is quite flat. On the other hand, recent results of microwave cavity resonance experiments[10] suggest that λ_c^{-2} drops very quickly from its zero-temperature value.

In this paper, we are interested in examining a number of issues. The first is to understand the role that a second layer (representing the chains) would have on λ_{ab} for both *d*-wave and *s*-wave order parameters. The second is to actually compute λ_c, a property that has not been widely examined in the literature. In order to keep the model simple, we have assumed that our two types of layers are coherently coupled. There is evidence[11] that there is some form of (incoherent) Josephson coupling between the CuO_2 layers of adjacent cells, but as a first step we feel that our approach is useful. We have also assumed that the copper-oxide chains in the YBCO do not contain a pairing mechanism of their own but are, instead, driven superconducting by their proximity to the copper-oxide planes.

Models of this type are known as S/N models (S standing for the intrinsically superconducting layer and N indicating the intrinsically normal layer). Previous work on S/N models has involved discussions of the density of states,[12–17] the Raman spectra,[15] the Knight shift and NMR rate,[12] and the response to microwave and optical frequency fields in both the *ab* planes and the *c* direction[12,18]. A closely related model, which has been studied extensively, is the S/S' model, in which there are two or more superconducting layers in the unit cell.[16,19,20] There have also been recent microscopic calculations by Graf, Rainer, and Sauls[21] and Radtke, Lau, and Levin[22] of the *c*-axis response in Josephson-coupled systems with a single layer type.

In this article we break the discussion down as follows: In Sec. II, we introduce the S/N model we use for our system. In Sec. III we derive an expression for the penetration depth and in Sec. IV we present the results of numerical calculations and discuss them qualitatively. In Sec. V we conclude with a comparison of our results with experiment.

II. THE MODEL

In this section we introduce a model on which we shall base our calculation of the penetration depth. The model is similar to one proposed by Abrikosov[15] and we have discussed many of its properties elsewhere.[17] In this model we consider two types of metallic layers, stacked alternately one above the other in the z direction. One of the layer types (S) contains a BCS-like pairing interaction, making the layer intriniscally superconducting. The other layer type (N) is intrinsically normal since it contains no pairing interaction, although it is driven superconducting by its proximity with the S layers. These layers form two sublattices which we assume to be weakly coupled to each other. The Hamiltonian is

$$\mathbf{H}-\mathbf{N}\mu=\sum_{\mathbf{k}\sigma}\left[\mathbf{c}^{\dagger}_{1\mathbf{k}\sigma}\mathbf{c}_{1\mathbf{k}\sigma}\xi_1(\mathbf{k})+\mathbf{c}^{\dagger}_{2\mathbf{k}\sigma}\mathbf{c}_{2\mathbf{k}\sigma}\xi_2(\mathbf{k})\right]+\sum_{\mathbf{k}\sigma}\left[t(\mathbf{k})\mathbf{c}^{\dagger}_{1\mathbf{k}\sigma}\mathbf{c}_{2\mathbf{k}\sigma}+t^{*}(\mathbf{k})\mathbf{c}^{\dagger}_{2\mathbf{k}\sigma}\mathbf{c}_{1\mathbf{k}\sigma}\right]-\sum_{\mathbf{k}}\left[\Delta_{\mathbf{k}}\mathbf{c}^{\dagger}_{1\mathbf{k}\uparrow}\mathbf{c}^{\dagger}_{1-\mathbf{k}\downarrow}+\Delta^{*}_{\mathbf{k}}\mathbf{c}_{1-\mathbf{k}\downarrow}\mathbf{c}_{1\mathbf{k}\uparrow}\right] \quad (1)$$

with $\mathbf{c}_{i\mathbf{k}\sigma}$ being the annihilation operator of an electron of spin σ and wave vector $\mathbf{k}$ in the ith sublattice. The in-plane dispersions are given by tight-binding dispersions

$$\xi_i=-2\sigma_i[\cos(k_x)+\cos(k_y)]-\mu_i, \quad (2)$$

where μ_i are the layer chemical potentials. When $\mu_1\neq\mu_2$, we have absorbed an offset in the band energies into the chemical potential. The sublattices are coupled with strength

$$t(\mathbf{k})=t_0\cos(k_z/2). \quad (3)$$

The Brillouin zone is $-\pi<k_x,k_y,k_z<\pi$. The form of Eq. (3) comes from assuming that the electrons are tightly bound to evenly spaced planes. The order parameter $\Delta_{\mathbf{k}}$ satisfies the usual BCS-like equation:

$$\Delta_{\mathbf{k}}\equiv\frac{1}{\Omega}\sum_{\mathbf{k}'}V_{\mathbf{k}\mathbf{k}'}\langle\mathbf{c}_{1-\mathbf{k}'\downarrow}\mathbf{c}_{1\mathbf{k}'\uparrow}\rangle, \quad (4)$$

where Ω is the volume of the crystal. We take the pairing potential to be separable for simplicity, so that $V_{\mathbf{k}\mathbf{k}'}=V\eta_{\mathbf{k}}\eta_{\mathbf{k}'}$ with $\eta_{\mathbf{k}}=1$ for an s-wave superconductor and $\eta_{\mathbf{k}}=\cos(k_x)-\cos(k_y)$ for a $d_{x^2-y^2}$ superconductor. In this case, we can write,

$$\Delta_{\mathbf{k}}=\Delta_0\eta_{\mathbf{k}}, \quad (5)$$

and solve Eq. (4) for Δ_0 instead of $\Delta_{\mathbf{k}}$. In the calculations presented in Sec. IV, we solve Eq. (4) for Δ_0 for each different set of band parameters.

If we choose to work in the Nambu representation, then we can write our Hamiltonian as

$$\mathbf{H}-\mathbf{N}\mu=\sum_{\mathbf{k}}\mathbf{C}^{\dagger}(\mathbf{k})Q(\mathbf{k})\mathbf{C}(\mathbf{k})+\text{const}\ , \quad (6)$$

where

$$\mathbf{C}(\mathbf{k})=\begin{bmatrix}\mathbf{c}_{1\mathbf{k}\uparrow}\\ \mathbf{c}^{\dagger}_{1-\mathbf{k}\downarrow}\\ \mathbf{c}_{2\mathbf{k}\uparrow}\\ \mathbf{c}^{\dagger}_{2-\mathbf{k}\downarrow}\end{bmatrix} \quad (7)$$

and

$$Q=\begin{bmatrix}\xi_1(\mathbf{k}) & -\Delta_{\mathbf{k}} & t(\mathbf{k}) & 0\\ -\Delta^{*}_{\mathbf{k}} & -\xi_1(-\mathbf{k}) & 0 & -t^{*}(-\mathbf{k})\\ t^{*}(\mathbf{k}) & 0 & \xi_2(\mathbf{k}) & 0\\ 0 & -t(-\mathbf{k}) & 0 & -\xi_2(-\mathbf{k})\end{bmatrix}. \quad (8)$$

Diagonalization of this Hamiltonian leads to the four bands $E_1=E_+$, $E_2=E_-$, $E_3=-E-$, $E_4=-E+$ with

$$E^2_{\pm}=\frac{\xi^2_1+\xi^2_2+\Delta^2_{\mathbf{k}}}{2}+t^2\pm\sqrt{\left[\frac{\xi^2_1-\xi^2_2+\Delta^2_{\mathbf{k}}}{2}\right]^2+t^2[(\xi_1+\xi_2)^2+\Delta^2_{\mathbf{k}}]}\ . \quad (9)$$

The Hamiltonian can then be written

$$\mathbf{H}-\mathbf{N}\mu=\sum_{\mathbf{k}}\sum_{i=1}^{4}\hat{\mathbf{C}}^{\dagger}_i(\mathbf{k})\hat{\mathbf{C}}_i(\mathbf{k})E_i(\mathbf{k})+\text{const}\ , \quad (10)$$

where $\hat{\mathbf{C}}_i(\mathbf{k})$ is the quasiparticle annihilation operator associated with the ith energy band. The operator, $\hat{\mathbf{C}}_i(\mathbf{k})$, is defined by

$$\hat{\mathbf{C}}_i(\mathbf{k})=\sum_{j=1}^{4}U^{\dagger}_{ij}(\mathbf{k})\mathbf{C}_j(\mathbf{k}), \quad (11)$$

and $U(\mathbf{k})$ is the 4×4 matrix which diagonalizes Q: $U_{ij}=U_i(E_j)$ with

$$U_i(E_j)=\frac{1}{\sqrt{C}}\begin{bmatrix}(E_j-\xi_2)A\\ -(E_j+\xi_2)B\\ tA\\ tB\end{bmatrix}, \quad (12)$$

$$A=t^2-(\Delta_{\mathbf{k}}+E_j+\xi_1)(E_j+\xi_2)\ ,$$

$$B=t^2-(\Delta^{*}_{\mathbf{k}}+E_j-\xi_1)(E_j-\xi_2)\ ,$$

$$C=A^2[t^2+(E_j-\xi_2)^2]+B^2[t^2+(E_j+\xi_2)^2]\ .$$

Now that we have diagonalized the Hamiltonian, it is straightforward to find the single-particle temperature Green's functions which we shall need in the following section. We have

$$G(\mathbf{k},\mathbf{k}';i\zeta_l)_{ij}=-\int_0^{\beta}d\tau\,e^{i\zeta_l\tau}\langle T\mathbf{C}_i(\mathbf{k};-i\tau)\mathbf{C}^{\dagger}_j(\mathbf{k}';0)\rangle$$

$$=\delta_{\mathbf{k},\mathbf{k}'}\sum_{m=1}^{4}\frac{U_{im}(\mathbf{k})U^{\dagger}_{mj}(\mathbf{k})}{i\zeta_l-E_m(\mathbf{k})}$$

$$\equiv\delta_{\mathbf{k},\mathbf{k}'}G(\mathbf{k};i\zeta_l)_{ij}\ , \quad (13)$$

where $\zeta_l=(2l+1)\pi/\beta$ are the fermion Matsubara frequencies, β is the inverse temperature, and T is the fermion time-ordered product.

III. PENETRATION DEPTH

In this section we follow the approach of Nam,[23] but with modifications to allow for the multiband nature of the problem. We begin with the expression for the current in a system generated by a weak applied magnetic vector potential, $A_\mu(\mathbf{q},\omega)$:

$$\langle J_\mu(\mathbf{r},\omega)\rangle = -\frac{n(\mathbf{r})e^2}{mc}A_\mu(\mathbf{r},\omega) - \frac{1}{c\Omega^2}\sum_{\nu,\mathbf{q},\mathbf{q}'} G^j_{R\mu\nu}(\mathbf{q},-\mathbf{q}',\omega)A_\nu(\mathbf{q}',\omega)e^{i\mathbf{q}\cdot\mathbf{r}} , \tag{14}$$

where the Greek subscripts refer to spatial directions, and $n \equiv \langle\Psi^\dagger\Psi\rangle$ is the electron density (Ψ are the field operators). $G^j_{R\mu\nu}(\mathbf{q},-\mathbf{q}',\omega)$ is the retarded current Green's function,

$$G^j_{R\mu\nu}(\mathbf{q},-\mathbf{q}',\omega) = -i\int_{-\infty}^{\infty} dt\, e^{i(\omega+i0^+)t} \times\langle[j_\mu(\mathbf{q},t), j_\nu(-\mathbf{q}',0)]\rangle\theta(t) \tag{15}$$

(with the square brackets indicating the commutator), and J_μ is the observable current operator,

$$J_\mu(\mathbf{r}) = j_\mu(\mathbf{r}) - \frac{e^2}{mc}\Psi^\dagger(\mathbf{r})\Psi(\mathbf{r})A_\mu(\mathbf{r}) \tag{16}$$

with

$$j_\mu = -\frac{e}{2m}\left\{\Psi^\dagger\left(-i\frac{\partial}{\partial x_\mu}\Psi\right) + \left(i\frac{\partial}{\partial x_\mu}\Psi^\dagger\right)\Psi\right\}. \tag{17}$$

The thermal average in Eq. (15) is taken with respect to the Hamiltonian in the absence of a perturbing field. As has been discussed at some length in the literature,[24] this means that Eq. (15) is not gauge invariant. However, provided that the applied field is along the *a*, *b*, or *c* axis, our expression for the current will be appropriate for the transverse gauge in which $\mathbf{q}\cdot\mathbf{A}(\mathbf{q},\omega) = 0$.

Rather than evaluate Eq. (15) directly, we evaluate the related temperature Green's function:

$$G^j_{\mu\nu}(\mathbf{q},\mathbf{q}',i\omega_l) = -\int_0^\beta d\tau\, e^{i\omega_l\tau}\langle T j_\mu(\mathbf{q},-i\tau)j_\nu(\mathbf{q}',0)\rangle. \tag{18}$$

In this expression, $\omega_l = 2l\pi/\beta$ are boson Matsubara frequencies, and T is the boson time-ordered product. In order to evaluate Eq. (18) it is necessary to find a useful form for $j_\mu(\mathbf{q})$. Unfortunately, this is not a simple matter for Bloch states when $\mathbf{q} \neq 0$. We can, however, use the properties of Bloch states to show that

$$j_\mu(\mathbf{q}) = e\sum_{\mathbf{k}} \mathbf{C}^\dagger(\mathbf{k})\gamma_\mu(\mathbf{k},\mathbf{k}+\mathbf{q})\mathbf{C}(\mathbf{k}+\mathbf{q}) , \tag{19}$$

where γ_μ is a vector of 4×4 matrices.

Using Eq. (19) we can evaluate the temperature Green's function to be

$$G^j_{\mu\nu}(\mathbf{q},\mathbf{q}',i\omega_l) = -\delta_{\mathbf{q},-\mathbf{q}'}\frac{e^2}{\beta}\sum_{n,\mathbf{k}} \mathrm{Tr}\left[G(\mathbf{k};i\zeta_n - i\omega_l)\gamma_\mu(\mathbf{k},\mathbf{k}+\mathbf{q})G(\mathbf{k}+\mathbf{q};i\zeta_n)\gamma_\nu(\mathbf{k}+\mathbf{q},\mathbf{k})\right] , \tag{20}$$

where the trace is over the components of the 4×4 matrix resulting from the product in the square brackets. Furthermore, we can substitute in for G using Eq. (13), then perform the sum over Matsubara frequencies and analytically continue $i\omega_l$ to the real axis to get

$$G^j_{R\mu\nu}(\mathbf{q},\mathbf{q}',\omega) = -\delta_{\mathbf{q},-\mathbf{q}'}e^2\sum_{i,j,\mathbf{k}} [\hat\gamma_\mu(\mathbf{k},\mathbf{k}+\mathbf{q})]_{ij}\,[\hat\gamma_\nu(\mathbf{k}+\mathbf{q},\mathbf{k})]_{ji}\,\frac{f[E_i(\mathbf{k})] - f[E_j(\mathbf{k}+\mathbf{q})]}{E_i(\mathbf{k}) - \omega - E_j(\mathbf{k}+\mathbf{q})}. \tag{21}$$

Here,

$$\hat\gamma_\mu(\mathbf{k},\mathbf{k}+\mathbf{q}) = U^\dagger(\mathbf{k})\gamma_\mu(\mathbf{k},\mathbf{k}+\mathbf{q})U(\mathbf{k}+\mathbf{q}), \tag{22}$$

where U is the unitary matrix described by Eq. (12). The $\mathbf{q}\to0$ limit of Eq. (21) has been discussed in Refs. 12 and 18.

The penetration depth can be found by evaluating Eq. (14) in the limit $\omega\to0$. Furthermore, since the high-T_c materials are in the London limit, we can let $\mathbf{q}\to0$:

$$\langle J_\mu(\mathbf{r},0)\rangle = -\frac{n(\mathbf{r})e^2}{mc}A_\mu(\mathbf{r},0) + \frac{1}{c\Omega}\sum_\nu G^j_{R\mu\nu}(0,0;0)A_\nu(\mathbf{r},0). \tag{23}$$

The first term, $-(ne^2/mc)A_\mu$, is most easily evaluated[23] by noting that $\langle J\rangle$ must vanish in the normal state. Then

$$\langle J_\mu(\mathbf{r},0)\rangle = -\sum_\nu K_{\mu\nu}A_\nu(\mathbf{r};0), \tag{24a}$$

with

$$K_{\mu\nu} = \frac{1}{c\Omega}\left\{G^j_{R\mu\nu}(0,0;0)\Big|_{\Delta=0} - G^j_{R\mu\nu}(0,0;0)\right\} \tag{24b}$$

and

$$G^j_{R\mu\nu}(0,0;0) = -e^2\sum_{i,j,\mathbf{k}} [\hat\gamma_\mu(\mathbf{k},\mathbf{k})]_{ij}\,[\hat\gamma_\nu(\mathbf{k},\mathbf{k})]_{ji} \times\left[\delta_{i,j}\frac{\partial f(E_i)}{\partial E_i} + [1-\delta_{i,j}]\frac{f(E_i)-f(E_j)}{E_i-E_j}\right]. \tag{24c}$$

Equation (24c) is one of the main results of this paper. It differs from the usual expression for the current Green's function by an important interband term (the second term in the square brackets). We will discuss this in some detail in the following section.

If $K_{\mu\nu}$ is diagonal in μ and ν, then the penetration depth λ_μ of a field aligned with one of the crystal axes into a large crystal face whose normal is along a crystal

axis, is

$$\frac{1}{\lambda_\mu^2} = \frac{4\pi}{c} K_{\mu\mu}. \tag{25}$$

In order to generate numerical results for Eq. (25), however, we need explicit expressions for $\gamma_\mu(\mathbf{k},\mathbf{k})$.

The matrices, $\gamma_\mu(\mathbf{k},\mathbf{k})$, will be determined by an approach which is suitable for the extreme tight-binding limit.[25] This is necessary because the usual technique, which notes that for Bloch states

$$-\frac{i}{m}\int d^3r\, \phi^*_{n\mathbf{k}} \nabla \phi_{n\mathbf{k}} = \frac{\partial \xi_n(\mathbf{k})}{\partial \mathbf{k}}, \tag{26}$$

cannot account for interband transitions ($n \neq n'$). The method we use for evaluating γ_μ begins with the recognition that

$$j_\mu(\mathbf{q}=0) = ie[\mathbf{H^n}, \mathbf{P}_\mu] \tag{27}$$

where $\mathbf{H^n}$ is the normal-state Hamiltonian [Eq. (1) with $\Delta_\mathbf{k} = 0$] and $\mathbf{P}_\mu$ is the polarization operator

$$\mathbf{P}_\mu = \int d^3r\, \Psi^\dagger(\mathbf{r}) r_\mu \Psi(\mathbf{r}). \tag{28}$$

Equation (27) effectively amounts to replacing ∇ with $[\nabla^2/2, \mathbf{r}]$ in $j(\mathbf{r})$. In the tight-binding limit, this allows us to make an important simplifying approximation. We write (suppressing spin for the moment)

$$\mathbf{P}_\mu \sim \sum_{i=1,2}\sum_{\mathbf{R}_i} R_{i\mu} \mathbf{c}_i^\dagger(\mathbf{R}_i)\mathbf{c}_i(\mathbf{R}_i), \tag{29}$$

where $\mathbf{c}_i^\dagger(\mathbf{R}_i)$ creates an electron in the Wannier state located at the sublattice point $\mathbf{R}_i$. The subscript i refers to the two possible sublattices. The operators $\mathbf{c}_i(\mathbf{R}_i)$ and $\mathbf{c}_i(\mathbf{k})$ are related via

$$\mathbf{c}_i(\mathbf{R}_i) = \frac{1}{N}\sum_\mathbf{k} e^{i\mathbf{k}\cdot\mathbf{R}_i}\mathbf{c}_i(\mathbf{k}), \tag{30}$$

where N is the number of lattice sites.

The normal-state Hamiltonian can also be expressed in terms of Wannier states:

$$\begin{aligned}\mathbf{H^n} = &-\sum_{i=1,2}\sum_{\mathbf{R}_i,\mathbf{d}} N\sigma_i \mathbf{c}_i^\dagger(\mathbf{R}_i+\mathbf{d})\mathbf{c}_i(\mathbf{R}_i) \\ &+\frac{Nt_0}{2}\sum_{\mathbf{R}_1}\Big[\mathbf{c}_1^\dagger(\mathbf{R}_1)\mathbf{c}_2(\mathbf{R}_1+\hat{\mathbf{z}}/2) \\ &+\mathbf{c}_1^\dagger(\mathbf{R}_1)\mathbf{c}_2(\mathbf{R}_1-\hat{\mathbf{z}}/2) + \text{H.c.}\Big].\end{aligned} \tag{31}$$

The vector $\mathbf{d}$ is the displacement to the nearest neighbors of $\mathbf{R}_i$ within the plane, $\hat{\mathbf{z}}$ is the unit vector in the z direction, and H.c. indicates the Hermitian conjugate. If we use Eqs. (29) and (31) in Eq. (27), we find that

$$\gamma_{\hat{\mathbf{x}}}(\mathbf{k},\mathbf{k}) = \begin{bmatrix} 2\sigma_1\sin(k_x) & 0 & 0 & 0 \\ 0 & 2\sigma_1\sin(k_x) & 0 & 0 \\ 0 & 0 & 2\sigma_2\sin(k_x) & 0 \\ 0 & 0 & 0 & 2\sigma_2\sin(k_x) \end{bmatrix}, \tag{32a}$$

$$\gamma_{\hat{\mathbf{y}}}(\mathbf{k},\mathbf{k}) = \begin{bmatrix} 2\sigma_1\sin(k_y) & 0 & 0 & 0 \\ 0 & 2\sigma_1\sin(k_y) & 0 & 0 \\ 0 & 0 & 2\sigma_2\sin(k_y) & 0 \\ 0 & 0 & 0 & 2\sigma_2\sin(k_y) \end{bmatrix}. \tag{32b}$$

Since there are no interlayer processes in $\gamma_{\hat{\mathbf{x}}}(\mathbf{k},\mathbf{k})$ and $\gamma_{\hat{\mathbf{y}}}(\mathbf{k},\mathbf{k})$, it is not surprising that their elements are the same as we would have found using Eq. (26). On the other hand, $\gamma_{\hat{\mathbf{z}}}(\mathbf{k},\mathbf{k})$ has only off-diagonal elements:

$$\gamma_{\hat{\mathbf{z}}}(\mathbf{k},\mathbf{k}) = \begin{bmatrix} 0 & 0 & \frac{-t_0}{2}\sin\left(\frac{k_z}{2}\right) & 0 \\ 0 & 0 & 0 & \frac{-t_0}{2}\sin\left(\frac{k_z}{2}\right) \\ \frac{-t_0}{2}\sin\left(\frac{k_z}{2}\right) & 0 & 0 & 0 \\ 0 & \frac{-t_0}{2}\sin\left(\frac{k_z}{2}\right) & 0 & 0 \end{bmatrix}. \tag{32c}$$

It is clear from the antisymmetric $\mathbf{k}$ dependence of γ_μ that $K_{\mu\nu}$ is, in fact, diagonal in μ and ν and, therefore, that λ_μ is given by Eq. (25).

IV. RESULTS AND DISCUSSION

We would like to begin this section with a discussion of Eqs. (24). In particular, Eq. (24c) differs from the well-known result for single-band materials by an additional term (the second term in the square brackets) which describes interband processes. This additional term is quite different from the intraband term (the first term in the square brackets) and is therefore worth examining in some detail. To begin with, we must understand that $G^j_{R\mu\nu}$, when evaluated in the superconducting state, describes paramagnetic processes that degrade the screening currents induced by the magnetic field.[23] This is quite clear in Eq. (24b), where the effect of $G^j_{R\mu\nu}$ is to reduce the magnitude of the kernel $K_{\mu\nu}$ and therefore increase the penetration depth.

The first term in $G^j_{R\mu\nu}$, which is proportional to

$\partial f(E_i)/\partial E_i$, describes the intraband paramagnetic response to an applied field. It accounts for the reduction of the superfluid density by the thermal excitation of quasiparticles. At $T = 0$ this term vanishes. As T increases, the number of excited quasiparticles will depend on the nature of the gap. For an isotropic s-wave gap, there will be an exponentially small number of excitations, and for a d-wave gap (which has nodes on the Fermi surface) there will be a linear increase in the number of quasiparticle excitations with temperature. The low-temperature dependence of the penetration depth in the ab plane has been taken as an important test of the symmetry of the gap for this reason.

The second term in $G^J_{R\mu\nu}$, which is proportional to $[f(E_i) - f(E_j)]/[E_i - E_j]$, describes two processes which contribute to the interband paramagnetic response. These processes are the transitions of electrons between the two electron bands, and the breaking of Cooper pairs in such a way that one electron finishes in each band. These two processes are best described in the quasiparticle picture where they can be understood as transitions between the four quasiparticle bands. The temperature dependence of these transitions depends on the relative signs of E_i and E_j. For example, $f(E_+) - f(E_-)$ vanishes at $T = 0$ and increases with T, while $f(E_+) - f(-E_-)$ is 1 at $T = 0$ and decreases with increasing T. Competition between these two terms leads to a flat low-T behavior whose specific features depend on the nature of the matrix elements $[\hat{\gamma}_\mu]_{ij}$. It is worth pointing out here that terms like $f(E_+) - f(-E_+)$ and $f(E_-) - f(-E_-)$ will not contribute to the paramagnetic response since $[\hat{\gamma}_\mu]_{14} = [\hat{\gamma}_\mu]_{41} = [\hat{\gamma}_\mu]_{23} = [\hat{\gamma}_\mu]_{32} = 0$. It should also be pointed out that the temperature dependence of the interband paramagnetic response is quite insensitive to the details of the gap structure, since the flat T dependence comes from the cancellation of an increasing function and a decreasing function which depend on the gap in similar fashions.

When we calculate the penetration depth using Eq. (25), then, we will find that the shape of the curves will be made up of contributions from both the intraband and interband paramagnetic processes. The relative strengths of the contributions will depend on the matrix elements of $\hat{\gamma}_\mu$. The significance of this point will become clear after we have presented the results of our calculations.

In Figs. 1 and 2, we plot the penetration depths as functions of temperature for two physically different limits of our model. These two limits were discussed at some length in a previous article,[17] where we found that despite the large number of free parameters in the Hamiltonian, the important factor determining the qualitative behavior of the model is the relative positioning of the Fermi surfaces in the Brillouin zone. In one limit, the Fermi surfaces of the two sublattices are far apart in the Brillouin zone. Since the interlayer coupling term in the Hamiltonian conserves $\mathbf{k}$, states near the Fermi surface in one sublattice will be coupled to states which are far from the Fermi surface of the other sublattice. Because of the large difference in energy of the states, the effect on the Fermi surfaces is perturbative. In the second limit, the Fermi surfaces of the two sublattices coincide in the Brillouin zone, and are directly coupled by the interlayer hopping. In this article we adjust the locations of the Fermi surfaces by varying μ_1 and μ_2, while holding the other band parameters fixed. In Fig. 1 we have graphed the penetration depths for an increasing sequence of interlayer coupling strengths t_0 in the limit of well separated Fermi surfaces. In Fig. 2, we consider the same range of t_0 values, but choose μ_1 and μ_2 such that the Fermi surfaces coincide.

First of all, in the case of well-separated Fermi surfaces (which is characterized by $|\mu_1\sigma_2 - \mu_2\sigma_1| \gg t_0^2$) the most important effect near the Fermi surface is the opening of an induced gap in the N sublattice. In Fig. 3 we plot the density of states in the S and N sublattices and the small induced gap in the N sublattice is clear. The magnitude of the gap is (for small t_0)

$$\epsilon_{\mathbf{k}} \sim \Delta_{\mathbf{k}} \left[\frac{\sigma_2 t(\mathbf{k})}{\mu_2\sigma_1 - \mu_1\sigma_2} \right]^2 \tag{33}$$

where $\mathbf{k}$ must be chosen to lie on the Fermi surface of the N sublattice. The maximum value of the gap on the Fermi surface is

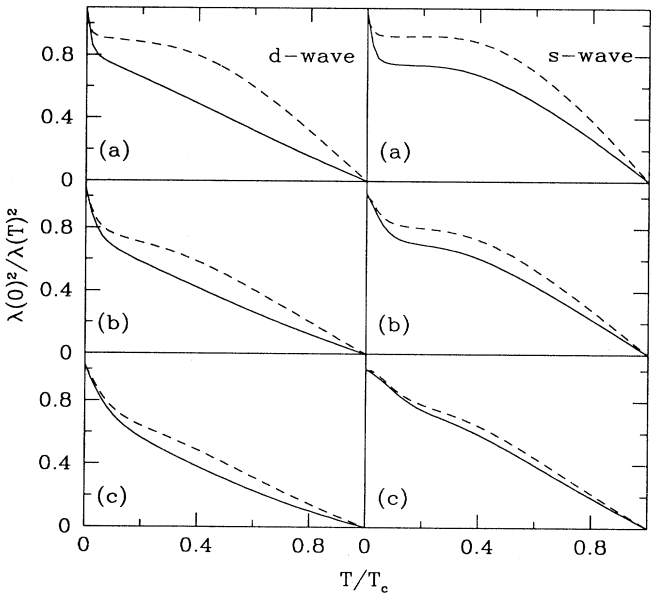

FIG. 1. Penetration depth for a series of interlayer coupling strengths. In these figures, the Fermi surfaces of the S and N sublattices are far apart in the Brillouin zone. The solid lines are for λ_{ab} and the dashed lines are for λ_c. The left-hand column is for a d-wave order parameter, and the right-hand column is for an s-wave order parameter. The coupling strengths are (a) $t_0 = 10$ meV, (b) 20 meV, and (c) 40 meV. The approximate energies of the induced gaps are, for d wave, (a) $\epsilon_0/T_c \sim 0.07$, (b) $\epsilon_0/T_c \sim 0.30$, (c) $\epsilon_0/T_c \sim 1.3$, and for s wave, (a) $\epsilon_0/T_c \sim 0.06$, (b) $\epsilon_0/T_c \sim 0.27$, (c) $\epsilon_0/T_c \sim 1.2$. The order parameter Δ_0 is determined from the BCS equation for each case. The band parameters are $\sigma_1 = 100$ meV, $\sigma_2 = 60$ meV, $\mu_1 = \mu_2 = -80$ meV and $T_c = 8.6$ meV $= 100$ K.

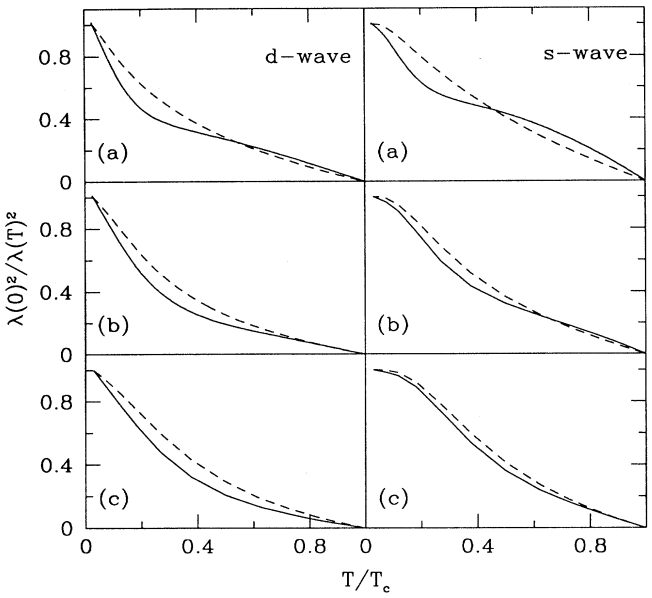

FIG. 2. Penetration depth for a series of coupling strengths. In these figures, the Fermi surfaces of the S and N sublattices are coincident. The solid lines are for λ_{ab}, while the dashed curves are for λ_c. Again, the left column is for a d-wave order parameter, while the right column is for an s-wave order parameter. The progression of coupling strengths is (a) $t_0 = 10$ meV, (b) 20 meV, and (c) 40 meV. The order parameter Δ_0 is determined from the BCS equation for each case. The band parameters are $\sigma_1 = 100$ meV, $\sigma_2 = 60$ meV, $\mu_1 = -80$ meV, $\mu_2 = -48$ meV, and $T_c = 8.6$ meV = 100 K.

$$\epsilon_0 \sim 2\Delta_0 \left[\frac{\sigma_2 t_0}{\mu_2\sigma_1 - \mu_1\sigma_2}\right]^2 \left[1 - \frac{|\mu_2|}{4\sigma_2}\right] \tag{34a}$$

for a d-wave gap and

$$\epsilon_0 \sim \Delta_0 \left[\frac{\sigma_2 t_0}{\mu_2\sigma_1 - \mu_1\sigma_2}\right]^2 \tag{34b}$$

for an s-wave gap. The energy ϵ_0 provides a temperature scale on which we see structure in $\lambda(T)$. The temperature $T = \epsilon_0$ is (roughly) the temperature at which a large fraction of the superfluid in the N sublattice is thermally depleted. In the relatively weakly coupled cases of Figs. 1(a) and 1(b), there is a sharp kink in both $\lambda_{ab}(T)^{-2}$ and $\lambda_c(T)^{-2}$ at $T \sim \epsilon_0$. On the other hand, in Fig. 1(c) where the interlayer coupling is stronger, ϵ_0 is of the order of T_c and we no longer see any definite structure associated with it.

This kind of multiple-gap structure also exists in the case where the Fermi surfaces of the sublattices coincide (for which $\mu_1\sigma_2 = \mu_2\sigma_1$). There are some important differences here, however. The main point is that the direct coupling of the Fermi surfaces through $t(\mathbf{k})$ leads to a strong hybridization of the Fermi surfaces of the two sublattices. Not surprisingly, the gap structure in the neighborhood of the Fermi surface is somewhat different than in the perturbative case. For example, in Fig. 4, where we have plotted the density of states for a d-wave order parameter, we see that there is a nested gap structure in which the outer gap can be identified with the order parameter and the inner gap is the result of the interference of the interlayer coupling and the order parameter. We have discussed this gap quantitatively elsewhere,[17] but because of the complexity of the discussion we will only repeat the most important points here. The first point to note is that the energy scale of the inner gap in Fig. 4 is much larger than that of the induced gap of Fig. 3 even though t_0 is larger in Fig. 3. In Fig. 2, we see that it is only for the smallest value of t_0 that there is a kink in the penetration depth that can be associated with the inner gap. For the larger values of t_0 the energy of the inner gap is larger than T_c. The second point about choosing coincident Fermi surfaces is that the Fermi surfaces become hybridized so that the inner gap cannot be thought of as an induced gap in the N sublattice, and must be treated as a gap in the hybridized band. This point is clear in Fig. 4 since the inner gap structure appears in both sublattice densities of states.

Besides the occurrence of kinks in the penetration depth curves, the most interesting feature of our graphs is the large difference in $\lambda_{ab}(T)$ and $\lambda_c(T)$. In Fig. 1(a), for the case of the d-wave order parameter, $\lambda_{ab}(T)^{-2}$ becomes very linear for $T > \epsilon_0$. This is the kind of behavior found in the usual two-dimensional d-wave superconductors.[7] Similarly, for the s-wave order param-

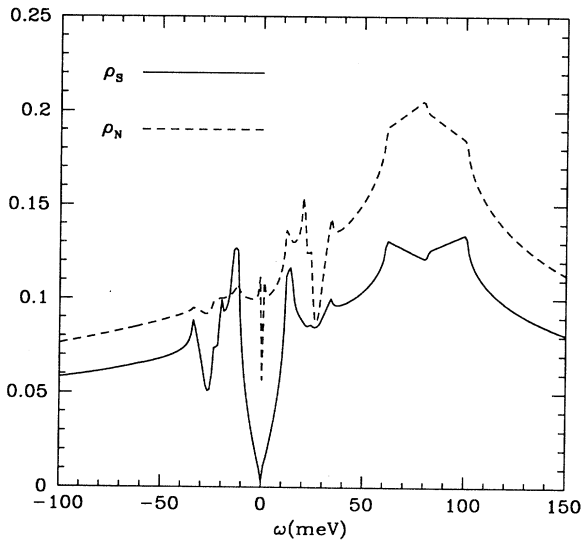

FIG. 3. Density of states for a d-wave order parameter. This plot is for the same band parameters as Fig. 1(b). Here we present the density of states of the S and N sublattices separately. We see that there is a small induced gap at the Fermi surface ($\omega = 0$ meV) in the N sublattice. The induced gap provides a second temperature scale (the first being T_c) over which we see structure in the penetration depth curves. The shape of the intrinsic gap in the S sublattice is perturbed only slightly by the interlayer coupling, so that once we are at temperatures above the energy scale of the induced gap, the penetration depth behaves qualitatively like the usual d-wave (or s-wave) case.

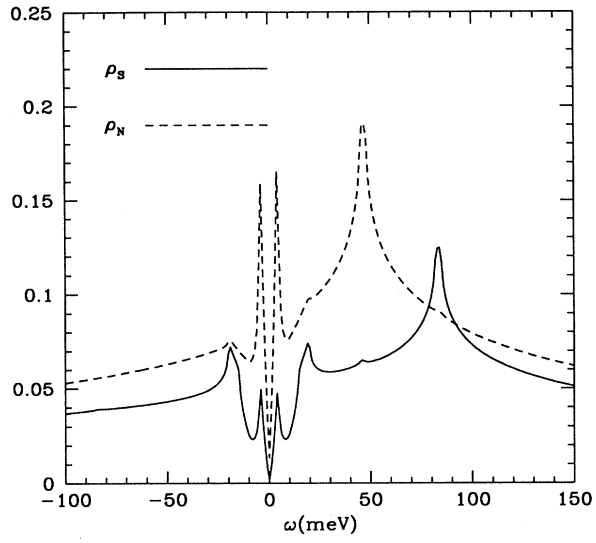

FIG. 4. Density of states for a *d*-wave order parameter. This plot is for the same band parameters as Fig. 2(a). Here there is a nested gap structure at the Fermi surface. The inner gap is shared between the two sublattices evenly, unlike in Fig. 3, and is the result of a complicated interference of $t(\mathbf{k})$ and $\Delta_{\mathbf{k}}$. The outer gap structure can be identified with $\Delta_{\mathbf{k}}$, though it becomes less prominent for larger values of t_0. What is important about this curve is that the size of the inner gap is comparable to T_c, even for weak interlayer coupling. The shape of the penetration depth curves, then, will be determined, not by the symmetry of $\Delta_{\mathbf{k}}$, but by the structure of the inner gap.

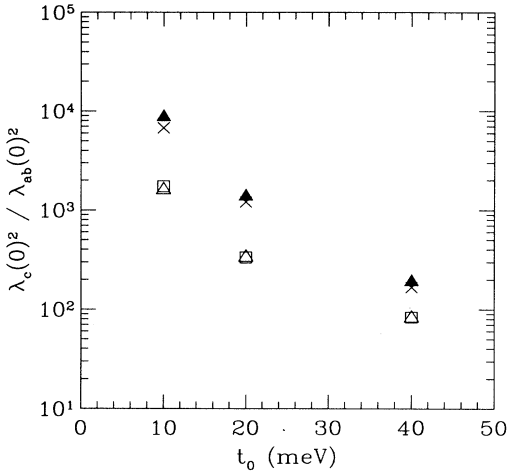

FIG. 5. Anisotropy ratios $\lambda_c(0)^2/\lambda_{ab}(0)^2$ for the four sets of data presented in Figs. 1 and 2. The solid triangles and crosses are for the *d*-wave and *s*-wave results of Fig. 1, respectively, and the open triangles and open squares are for the *d*-wave and *s*-wave results of Fig. 2. The observed anisotropy in $YBa_2Cu_3O_{6.95}$ is ~ 50.

eter, $\lambda_{ab}(T)^{-2}$ appears to have an exponential behavior for $T > \epsilon_0$. On the other hand, $\lambda_c(T)^{-2}$ has a very flat behavior for intermediate values of $T > \epsilon_0$ in both cases. From our discussion of the paramagnetic terms in Eq. (24c), it is clear that the intraband terms must be dominating the behavior of the *ab*-plane penetration depths and that the interband terms determine the low-temperature behavior of the *c*-axis penetration depth. We could see this directly by calculating the relative sizes of the matrix elements of $[\hat{\gamma}_\mu]_{ij}$, but it is sufficient to note that for small t_0, the unitary matrices U mix the two sublattices weakly, and that $\hat{\gamma}_\mu$ will differ from γ_μ by terms of order $t^2/|\xi_1^2 - \xi_2^2|$ (our assumption that the sublattice Fermi surfaces are well separated ensures that this is small). What this is saying is that, in the weakly coupled limit, currents which are confined to within a plane, are also approximately confined to within a band. Similarly, currents along the *c* axis, for which electrons must hop between the two sublattices, are mostly described by interband transitions.

As t_0 is increased, however, the bands will begin to lose their sublattice character. In this case the penetration depths will depend on both interband and intraband processes. We can see this in Fig. 1. As t_0 increases, $\lambda_{ab}(T)^{-2}$ and $\lambda_c(T)^{-2}$ become increasingly similar in shape. In the case of the *d*-wave order parameter, for example, we can see that λ_c starts to show a linear behavior which is a reflection of the symmetry of the gap. This is also what we find in the *s*-wave case, although it must be remembered that for large couplings, the gap which determines the overall shape of the penetration depth is $\epsilon_{\mathbf{k}}$ [Eq. (33)], and that $\epsilon_{\mathbf{k}}$ has a node $k_z = \pm\pi$ due to its dependence on $t(\mathbf{k})$. In Fig. 1(c), this node makes $\lambda_{ab}(T)$ virtually indistinguishable from the usual two-dimensional *d*-wave case.

If the Fermi surfaces of the sublattices are coincident, then the hybridization of the sublattices makes it impossible to associate bands with layers. In this case, both λ_{ab} and λ_c will depend on both intraband and interband processes. In Fig. 2, $\lambda_{ab}(T)^{-2}$ and $\lambda_c(T)^{-2}$ have similar shapes, even for the weakest interlayer couplings. The node in $t(\mathbf{k})$ has introduced a node in the inner gap[17] which changes the exponential low-temperature behavior of the *s*-wave case to a linear behavior.

We finish this section with a brief discussion of the anisotropy ratio $\lambda_c(0)^2/\lambda_{ab}(0)^2$. In Fig. 5 we plot the anisotropies for the four different cases we have run. We can see that the anisotropy is relatively insensitive to the order parameter, but depends quite strongly on the coupling strength and the choice of band parameters. In the paper of Basov *et al.*,[9] they find $\lambda_c(0) \sim 1\,\mu$m in $YBa_2Cu_4O_8$, and we take $\lambda_{ab}(0) \sim 0.14\,\mu$m so that the anisotropy ratio is $\lambda_c(0)^2/\lambda_{ab}(0)^2 \sim 50$. This would suggest that, from Fig. 5, we need to have interlayer couplings of the order of 50 meV. If we compare this with the size of the in-plane nearest-neighbor coupling energies, $\sigma_i \sim 100$ meV, we see that two sublattices can no longer be considered weakly coupled.

V. CONCLUSIONS

The main results of this article are the following.

(i) An expression [Eq. (24c)] for the penetration depth which differs from the usual expression by a term which

accounts for interband transitions. The temperature dependence of this term is quite different from that of the usual penetration-depth expression, and we use this fact to explain the very flat low-temperature behavior of λ_c^{-2} seen in Figs. 1(a) and 1(b). A further feature of this interband term is that it is only weakly sensitive to the symmetry of the order parameter.

(ii) Calculations of the penetration depths, λ_{ab} and λ_c for a layered S/N model in which we identify two important physical limits. In the first limit, the Fermi surfaces of the S and N layers are far apart in the Brillouin zone and are only modified perturbatively by the interlayer coupling. In the second limit, the Fermi surfaces coincide and form a strongly hybridized state. The difference between the two cases shows up in the gap structure. For the perturbative case there is a weak, induced gap in the S sublattice which appears as a sharp kink at low temperature in the penetration depths. For the hybridized limit, the gap structure has a larger energy scale (of the order of T_c) so that there is no obvious structure apparent in the penetration depths.

(iii) An increased understanding of the role of the interlayer coupling between the S and N layers. As is well known, the interlayer coupling drives the N sublattice into the superconducting state by a proximity effect, but also serves to reduce the anisotropy of the system. It is for this reason that, as t_0 increases in Figs. 1 and 2, λ_{ab} and λ_c become increasingly similar. Our choice of $t(\mathbf{k})$ also introduces an additional $\mathbf{k}$ dependence into the gap structure. As we pointed out in our discussion, for example, this results in $\lambda_{ab}(T)$ for the s-wave case shown in Fig. 1(c) being indistinguishable from the usual two-dimensional d-wave case. The change in anisotropy that comes with changing t_0 is shown in Fig. 5. We concluded in Sec. IV that, in order for the anisotropy to agree with the experimental observations of $YBa_2Cu_3O_{6.95}$, fairly strong interlayer couplings are required.

There are several problems with the weakly coupled proximity effect model. We mentioned above that a weak interlayer coupling leads to a value of $\lambda_c(0)^2/\lambda_{ab}(0)^2$ which is much larger than observed by experiment. Another problem is the kinklike features, seen most clearly in Fig. 1, which are associated with the induced gap in the N sublattice. These have never been experimentally observed, to our knowledge. It is also not likely that these features just have not been observed because they occur at temperatures below the lowest values achieved in experiments (1.3 K[1]), since these kinks are associated with the depletion of the superfluid in the N sublattice. We know from the work of Basov *et al.* and Zhang *et al.*[8] that there is a substantial superfluid density in the copper-oxide chains at all $T < T_c$. This is unfortunate because the one promising feature of the weakly coupled proximity model is the flat low-T behavior of λ_c^{-2}.

If we look at larger interlayer coupling strengths, then we will have reasonable values for the anisotropy and a significant superfluid fraction in the N layers at all temperatures. On the other hand the behavior of $\lambda_c(T)$ becomes much like that of $\lambda_{ab}(T)$ and quite unlike that which is observed.

One possible modification to the model which might allow us to retain the flat, low-T behavior for λ_c^{-2}, would be to couple the chains to the planes incoherently. Radtke, Lan, and Levin[22] find that an intrinsically Josephson-coupled model, with one layer per unit cell, leads to a flat low-T behavior in λ_c^{-2}. We have also shown in this paper that the penetration depth depends strongly on the band structure. With this in mind, we feel that a second modification of the model which must be made is to include the one-dimensional nature of the chains. The obvious reason for this is to account for the observed ab-plane anisotropy. A less obvious reason is that the Fermi surfaces of the chains and planes will now cross, and will not simply belong to one of the two categories (weakly coupled or hybridized) described above. In order to make an accurate prediction of the penetration depth, it is necessary to use a band structure which describes the important features of the Fermi surface.

Following the initial submission of this article, we were made aware of a paper by Klemm and Liu,[26] in which the penetration depth of a layered S/N system is calculated. Their work is similar to what has been done here, and they arrive at an equation which is equivalent to Eq. (24c) for the penetration depth. There are some notable differences between their work and that which we have presented here: they restrict their order parameter to be s wave, and only consider the case when the two Fermi surfaces coincide. They present numerical results for a set of band parameters which have been fitted to experiment, and arrive at figures which are quantitatively similar to Fig. 2(c).

ACKNOWLEDGMENTS

We would like to thank D. N. Basov and T. Timusk for helpful discussions and for sharing their data prior to publication. This work was supported in part by the Natural Sciences and Engineering Council of Canada (NSERC) and the Canadian Institute for Advanced Research (CIAR).

[1] W. N. Hardy *et al.*, Phys. Rev. Lett. **70**, 3999 (1993).
[2] A. T. Fiory *et al.*, Phys. Rev. Lett. **61**, 1419 (1988).
[3] J. M. Pond *et al.*, Appl. Phys. Lett. **59**, 3033 (1991).
[4] D. A. Bonn *et al.*, Phys. Rev. B **47**, 11 314 (1993).
[5] J. Annett, N. Goldenfeld, and S. R. Renn, Phys. Rev. B **43**, 2778 (1991).
[6] M. Prohammer and J. P. Carbotte, Phys. Rev. B **43**, 5370 (1991).
[7] P. Arberg, M. Mansor, and J. P. Carbotte, Solid State Commun. **86**, 671 (1993).
[8] D. N. Basov *et al.*, Phys. Rev. Lett. **74**, 598 (1995); K. Zhang *et al.*, *ibid.* **73**, 2484 (1994).
[9] D. N. Basov, T. Timusk, B. Dabrowski, and J. D. Jorgensen, Phys. Rev. B **49**, 3511 (1994); C. C. Homes, T. Timusk, D. A. Bonn, R. Liang, and W. N. Hardy (unpublished).

[10] J. Mao, D. H. Wu, J. L. Peng, R. L. Greene, and S. M. Anlage, Phys. Rev. B **51**, 3316 (1995).
[11] R. Kleiner and P. Müller, Phys. Rev. B **49**, 1327 (1994).
[12] M. Tachiki, S. Takahashi, F. Steglich, and H. Adrian, Z. Phys. B **80**, 161 (1990); M. Tachiki, T. Koyama, S. Takahashi, Prog. Theor. Phys. Suppl. **108**, 297 (1992); S. Takahashi and M. Tachiki, Physica C **170**, 505 (1990).
[13] A. I. Buzdin, V. P. Damjanović, and A. Y. Simonov, Phys. Rev. B **45**, 7499 (1992); A. I. Buzdin, V. P. Damjanović, and A. Y. Simonov, Physica C **194**, 109 (1992).
[14] L. N. Bulaevskii and M. V. Zyskin, Phys. Rev. B **42**, 10 230 (1990).
[15] A. A. Abrikosov, Physica C **182**, 191 (1991); A. A. Abrikosov and R. A. Klemm, Physica C **191**, 224 (1992).
[16] V. Z. Kresin, Phys. Rev. B **25**, 157 (1982); V. Z. Kresin and S. A. Wolf, *ibid.* **46**, 6458 (1992); V. Z. Kresin, H. Morawitz, and S. A. Wolf, *Mechanisms of Conventional and High T_c Superconductivity* (Oxford University Press, Oxford, 1993).
[17] W. A. Atkinson and J. P. Carbotte, Phys. Rev. B **51**, 1161 (1995).
[18] A. Yu. Simonov, Physica C **211**, 455 (1993).
[19] S. H. Liu and R. A. Klemm, Phys. Rev. B **48**, 4080 (1993); **48**, 10 650 (1993), and references contained therein; S. H. Liu and R. A. Klemm, Physica C **216**, 293 (1993).
[20] S. Kettemann and K. B. Efetov, Phys. Rev. B **46**, 8515 (1992).
[21] M. J. Graf, D. Rainer, and J. A. Sauls, Phys. Rev. B **47**, 12 089 (1993).
[22] R. J. Radtke, C. N. Lau, and K. Levin (unpublished).
[23] S. B. Nam, Phys. Rev. **156**, 470 (1967).
[24] P. J. Hirschfeld and D. Einzel, Phys. Rev. B **47**, 8837 (1993); F. Gross *et al.*, Z. Phys. B **64**, 175 (1986); A. J. Millis, Phys. Rev. B **35**, 151 (1987).
[25] G. D. Mahan, *Many-Particle Physics* (Plenum, New York, 1986), p. 30.
[26] R. A. Klemm and S. H. Liu, Phys. Rev. Lett. **74**, 2343 (1995).